



Available online at [www.sciencedirect.com](http://www.sciencedirect.com)

**ScienceDirect**

[Advances in Space Research 60 \(2017\) 1644–1656](#)

**ADVANCES IN  
SPACE  
RESEARCH**  
(*a COSPAR publication*)  
[www.elsevier.com/locate/asr](http://www.elsevier.com/locate/asr)

# Vertical and oblique HF sounding with a network of synchronised ionosondes

Tobias Verhulst <sup>a,\*</sup>, David Altadill <sup>b</sup>, Jens Mielich <sup>c</sup>, Bodo Reinisch <sup>d,e</sup>, Ivan Galkin <sup>e</sup>, Angelos Mouzakis <sup>f</sup>, Anna Belehaki <sup>f</sup>, Dalia Burešová <sup>g</sup>, Stanimir Stankov <sup>a</sup>, Estefania Blanch <sup>b</sup>, Daniel Kouba <sup>g</sup>

<sup>a</sup> Royal Meteorological Institute (RMI), Ringlaan 3, Brussels B-1180, Belgium

<sup>b</sup> Observatori de l'Ebre (OE), Univ. Ramon Llull – CSIC, Horta Alta 38, 43520 Roquetes, Spain

<sup>c</sup> Leibniz-Institute of Atmospheric Physics at the University Rostock, Schlossstr. 6, Kuehlungsborn 18225, Germany

<sup>d</sup> Lowell Digisonde International, 175 Cabot Street, Lowell, MA 01854, USA

<sup>e</sup> University of Massachusetts Lowell, Space Science Laboratory, Lowell, MA 01854, USA

<sup>f</sup> National Observatory of Athens, IAASARS, Metaxa and Vas. Pavlou, Palai Penteli 15236, Greece

<sup>g</sup> Institute of Atmospheric Physics, Czech Academy of Sciences, Boční II 1401, 141 31 Prague, Czech Republic

Received 3 April 2017; received in revised form 10 May 2017; accepted 17 June 2017

Available online 23 June 2017

## Abstract

A network of ionosondes in Europe has been established to monitor travelling ionospheric disturbances (TIDs) by simultaneously making vertical and oblique incidence HF sounding measurements. This network is the outcome of the Net-TIDE project, a collaboration between European Digisonde operators that have synchronised the sounding schedules of the Digisondes in order to record vertical and oblique ionogram traces simultaneously, and have added Digisonde-to-Digisonde (D2D) fixed frequency oblique-incidence measurements to the measurement schedule. The distances between the observatories involved in the project range from 500 km to over 2000 km. The technical feasibility of this network approach is explored. The challenge for the fixed-frequency D2D skymap measurements is the automatic selection of the sounding frequencies depending on the geometry of the sounding paths, the diurnal and seasonal ionospheric changes, and space weather induced events.

© 2017 COSPAR. Published by Elsevier Ltd. All rights reserved.

**Keywords:** Travelling ionospheric disturbances; Digisonde; Oblique sounding

## 1. Introduction

Travelling Ionospheric Disturbances (TIDs) are the transient signatures in the ionosphere of propagating gravity waves, originating from various sources (Hines, 1974; Balthazar and Moffett, 1997; Hunsucker, 1982; Hocke and Schlegel, 1996; Astafyeva and Afraimovich, 2004). TIDs can significantly affect the operation of, for example,

high-frequency (HF) communication links, radio wave direction finding services, GNSS systems, and satellite communication by causing variations in the maximal usable frequency (*MUF*) and total electron content (*TEC*). Large scale TIDs (LSTIDs) can cause variations of up to 10 TECU in *TEC*, and of more than 1 MHz in *MUF* (e.g., Hernández-Pajares et al., 2006; MacDougall et al., 2009; Pintor et al., 2015). Despite several decades of investigation it is still unclear whether the LSTIDs are periodic processes or solitary waves (Hunsucker, 1982) propagating to large distances from the source of genera-

\* Corresponding author.

E-mail address: [tobias.verhulst@meteo.be](mailto:tobias.verhulst@meteo.be) (T. Verhulst).

tion, or what the form and the width of the wave front of LSTIDs is (Afraimovich et al., 2008). It is therefore important to monitor the ionosphere for the presence of TIDs. Currently, most TID detection techniques are based on *TEC* maps (Ho et al., 1998; Afraimovich et al., 2000; Hernández-Pajares et al., 2006; Ding et al., 2007; Borries et al., 2009). While these methods are useful for the detection especially of the large-scale TIDs, they have some serious limitations. The error in the vertical *TEC* maps is of the order of 3 TECU, i.e., of the same order as the variations caused by the TIDs. Secondly, the *TEC* variations only indicate the total, integrated effect of the disturbances, while many applications are primarily influenced by the variations in the bottom-side ionosphere. Other TID detection methods include using all-sky airglow imagers (e.g., Otsuka et al., 2009; Lakshmi Narayanan et al., 2014), especially for the lower regions of the ionosphere, or using the SuperDARN system at high latitudes (Frissell et al., 2014).

The Pilot Network for Identification of Travelling Ionospheric Disturbances (Net-TIDE project) (Belehaki et al., 2015; Reinisch et al., submitted for publication) proposes an alternative method for the detection and specification of TIDs, using bistatic oblique sounding between ionospheric observatories in Europe equipped with Digisonde DPS4D (Reinisch et al., 2009). On various links between two observatories, oblique single-frequency soundings are performed at regular time intervals, with usually one Digisonde transmitting and the other receiving the skywave signals. These oblique Digisonde-to-Digisonde (D2D) single-frequency skymap measurements provide the Doppler frequency, angle of arrival, and time of flight of the skywave signals. By using the Frequency & Angular Sounding (FAS) technique (Galushko et al., 2003; Paznukhov et al., 2012; Huang et al., 2016), information can be deduced from these measured signal characteristics about TIDs passing through the ionospheric reflection point, including their amplitude, speed, and direction of propagation.

The network of DPS4D observatories involved in the Net-TIDE project extends across Europe with ground-distances between the observatories from ~500 to ~2000 km (Fig. 1). All stations are equipped with the standard transmit and receive antennas, which are designed first and foremost for vertical incidence (VI) sounding, i.e., the oblique transmission is therefore fairly inefficient. To maintain a sufficiently high signal-to-noise ratio (SNR) for the fixed-frequency D2D skymap measurements, a prudent selection of the operating frequency must be done.

This paper investigates the challenges associated with producing high-quality oblique incidence (OI) sounding data on long paths, over 1000 km, without deployment of specialised Tx or Rx antennas, and without interrupting the routine VI ionogram and skymap measuring schedules at each observatory. In Section 2, the paper describes the synchronised operation between different Digisondes to produce combined ionograms showing both vertical and

oblique echo traces. We show first results obtained from these soundings, mainly discussing the operations on the link between the observatories at Dourbes (DB049; 50.1° N, 4.6°E) and Ebre (EB040; 40.8°N, 0.5°E). This link has a ground-distance of 1082 km (see Fig. 1).

In addition, we briefly discuss some of the challenges of receiving signals from a single transmitter at two receivers, and of receiving the transmissions from several stations at a single receiver. For the first case, we investigate the simultaneous reception of the signals from Dourbes at Ebre and Athens (AT138; 38.0°N, 23.5°E). The length of the Dourbes to Athens path is 2012 km (Fig. 1). For the second situation, we look at the reception of signals from Dourbes, Athens, and Pruhonice (PQ052; 50.0°N, 14.6°E) at Juliusruh (JR055; 54.6°N, 13.4°E).

In Section 3, we demonstrate how the measured oblique ionogram traces can be used to select the optimal frequency for the production of D2D skymaps, and how this frequency needs to be adapted to the time of day and season, to ionospheric storm conditions, and the prevailing radio spectrum pollution (interference). We then present some first measurements of the Doppler shift obtained from D2D skymaps. Section 4 presents a method of partial specification of the TID characteristics directly from the measured Doppler shift and *MUF* values, without involving the FAS technique.

## 2. Combined vertical and oblique ionogram sounding

While most ionosondes record VI ionograms, it has long been established that oblique ionograms can also be produced by synchronising the transmission and reception of spaced ionosondes (e.g., Reinisch et al., 1984a,b; Krasheninnikov et al., 1996; Zolesi et al., 2008). This can be done by running one ionosonde (Rx) in a “radio-quiet” mode, i.e., transmitter off, so that it only receives skywave signals from the remote transmitting station (Tx). The transmitting ionosonde on the other hand, sees only vertical incidence (VI) echo traces, and there are no oblique incidence (OI) signals that could confuse the automatic VI ionogram scaling (Galkin et al., 2008). Digisondes have, however, the advantage of automatically identifying signals arriving within zenith angles of less than 15° as VI (red for O-mode, green for X-mode), and those with zenith angles larger than 15° as OI (Fig. 2), and the automatic scaler can therefore reliably scale the VI echo traces by simply disregarding any signals flagged as OI. Both stations can therefore simultaneously register VI and OI traces in a combined “VI + OI” ionogram. Typical program settings for the DPS4Ds in the network are given in Table 1.

Oblique ionograms are essential for the selection of “optimal” sounding frequencies for the fixed-frequency skymap measurements for producing high-quality data for the TID diagnostics. Fig. 2 shows an example of the simultaneously recorded VI + OI ionograms recorded in Ebre and Dourbes. The traces below 8 MHz are the vertical



Fig. 1. Long distance oblique sounding links in the Net-TIDE network.

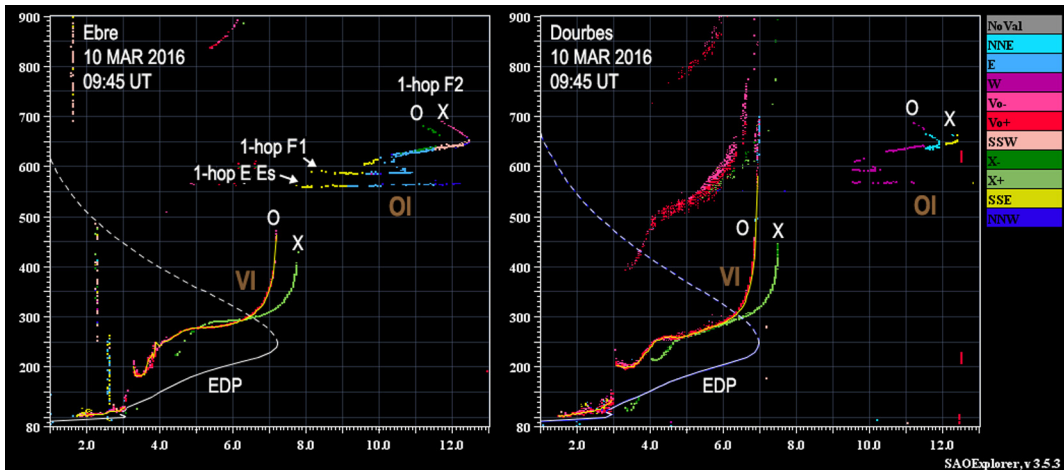


Fig. 2. VI + OI ionograms at Ebre (left) and Dourbes (right). The traces below 8 MHz are VI echoes (red = O polarisation, green = X polarisation); the traces between 8 MHz and 13 MHz are OI skywave signals transmitted by the other DPS4D. (For interpretation of the references to colour in this figure legend, the reader is referred to the web version of this article.)

Table 1

Typical Digisonde settings for combined VI and OI ionogram soundings. The limits of the frequency scan are indicative only, and are adapted to the diurnal/seasonal variations of the ionosphere (see LDI (2014) for detailed information on Digisonde configuration).

Program setting	VI + OI	D2D
Frequency	Scan, e.g., 1–16 MHz	Fixed, operator adjusted
Coarse step	50 kHz	—
Fine steps	2 steps, 5 kHz	—
Fine step multiplexing	Enabled	—
Integrated repeats	8	2048
Interpulse phase switching	Enabled	Disabled

echoes received at each station from its own transmissions. The signal traces between 9 MHz and 13 MHz are the oblique skywave signals received from the remote DPS4D. The vertical axis in the ionograms gives the virtual height  $h'(f) = \frac{1}{2} c \tau_o(f)$ , where  $c$  is the free-space speed of light, and  $\tau_o$  the time of flight of the HF pulses. The electron density profile (EDP) (e.g., Reinisch and Huang, 1983) is calculated from the  $h'(f)$  traces, and gives the real or “true” reflection heights. The “virtual range”  $r'(f) = c\tau_o$  to the reflection point (~mid-point) for the oblique signal is given by  $r'(f) = \sqrt{[(D/2)]^2 + [h'(f)]^2}$ , where  $\tau_o$  is the measured time of flight of the oblique signal, and  $D$  the distance between Tx and Rx (if  $D$  is measured in a straight line; otherwise the curvature of the earth has to be taken into account). The oblique signals are reflected in the  $E$  region ( $E$  or  $Es$  layer), the  $F_1$  region, and the  $F_2$  region as indicated in the left panel of Fig. 2.

Fig. 3 shows a series of oblique ionograms recorded at Juliusruh, listening in radio-quiet mode to the transmissions from Pruhonice (517 km) (left panel), from Dourbes (778 km) and Athens (2011 km) (middle panel), and from Athens (right panel). The respective traces, formed by the different oblique skywave signals, can be easily identified because of their different virtual ranges, and their different “nose” frequencies. At the nose frequency, the virtual range of the high-angle or Pedersen ray and the low angle ray become equal (e.g., Davies, 1990; de Boer, 2013); this is essentially the maximum-useable-frequency, MUF, as illustrated in Fig. 4. The colours for the oblique traces in Figs. 2 and 3 should show the approximate azimuth angle (with 60° resolution) of the arriving signals, according to the given colour code. This colour indication works reliably, however, only for frequencies below ~5 MHz, as demonstrated in Fig. 3 for the signals from Pruhonice (SSE) and Dourbes (W and SSW). For higher frequencies,  $2\pi$  ambiguities of the phase differences measured at the four antennas of the Digisonde's receiver antenna array result in erroneous azimuth angles (colours), as clearly seen in the Athens signal traces in Fig. 3. The Athens signals are actually arriving at Juliusruh from ~SSE, and the trace should be yellow for all trace points, but is not. The 2-s off-

set of the ionogram starting times from the full minute was introduced to avoid “interference” in the ionograms of the other network stations, which start at the full minute.

### 3. Selecting the D2D sounding frequencies

Judicious selection of the operating fixed frequency for every D2D link is required for routine TID monitoring. The frequency for each link should be as high as possible to minimise the nondeviative absorption in the D region (during daytime), but it must be smaller than the maximum usable frequency (MUF) prescribed by the prevailing ionospheric conditions. In addition, the selected frequency slots should not be occupied by strong nearby HF radio transmissions that would adversely affect the signal-to-noise ratio (SNR) of the D2D data.

#### 3.1. Oblique sounding Dourbes to Ebre

Using the MUF frequencies predicted by ionospheric models, like the International Reference Ionosphere (IRI) model (Bilitza et al., 2014) and various other median or nowcasting models (Zolesi et al., 2008), proved to be inadequate. Instead, the Net-TIDE project derives the sounding frequencies for each link by evaluating the diurnal variations of the SNR at each frequency in the sequence of OI ionograms. Digisonde ionograms measure the signal amplitude, Amp, and determine for each frequency the most probable amplitude, MPA, from the distribution of amplitudes for all ranges. The SNR is then defined as  $\text{SNR} [\text{dB}] = \text{Amp}-\text{MPA}$ . Fig. 5 is a typical example of the diurnal variation, depicting the SNRs for a 24-h period on 1 April 2016, with data from OI ionograms at Ebre for the Dourbes–Ebre link. The selected optimal sounding frequencies for night-time, twilight, and daytime are indicated in red. Note that the twilight period is only ~120 min long because of the steep nighttime ↔ daytime transitions. Selecting a different sounding frequency for such short time period is however detrimental of making continuous TID observations. The FAS analysis in the Net-TIDE project uses a sliding 160-min time window for the spectral analysis

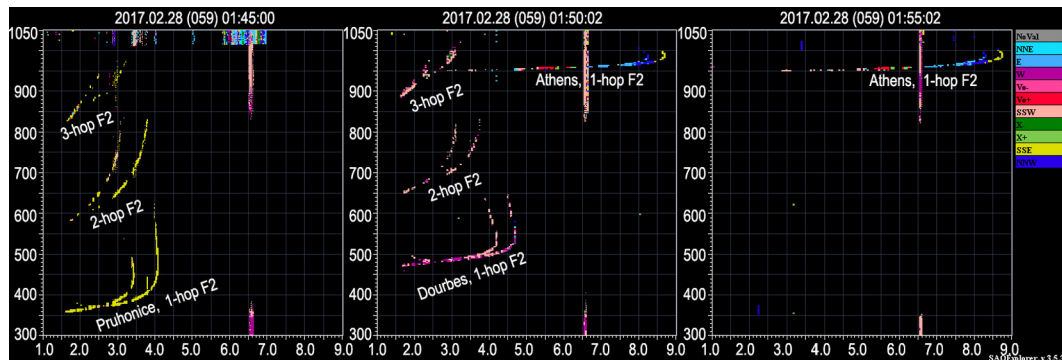


Fig. 3. Oblique signal traces recorded with the Juliusruh Digisonde operating in radio-quiet mode on 28 February 2017 at 01:45:00 UT (left), 01:50:02 UT (middle), and 01:55:02 UT (right).

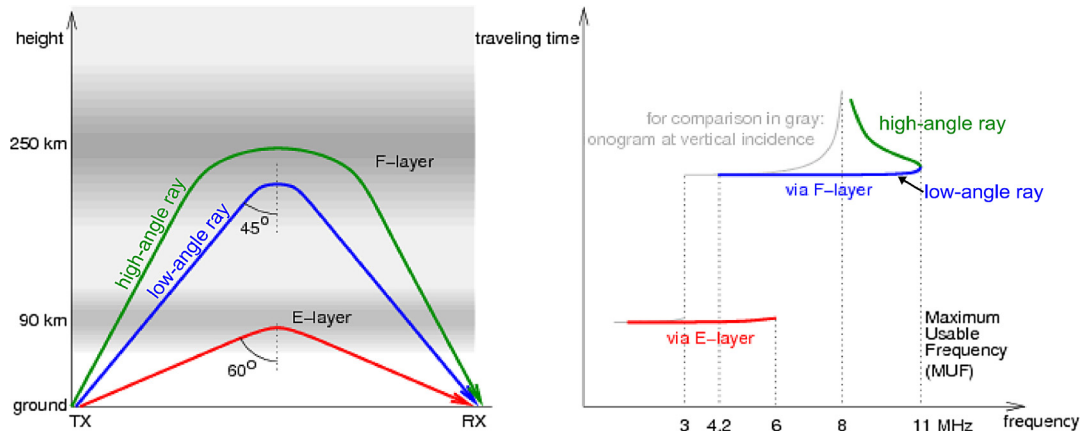


Fig. 4. Schematic representation of the different propagation modes for OI ionograms [after de Boer, 2013].

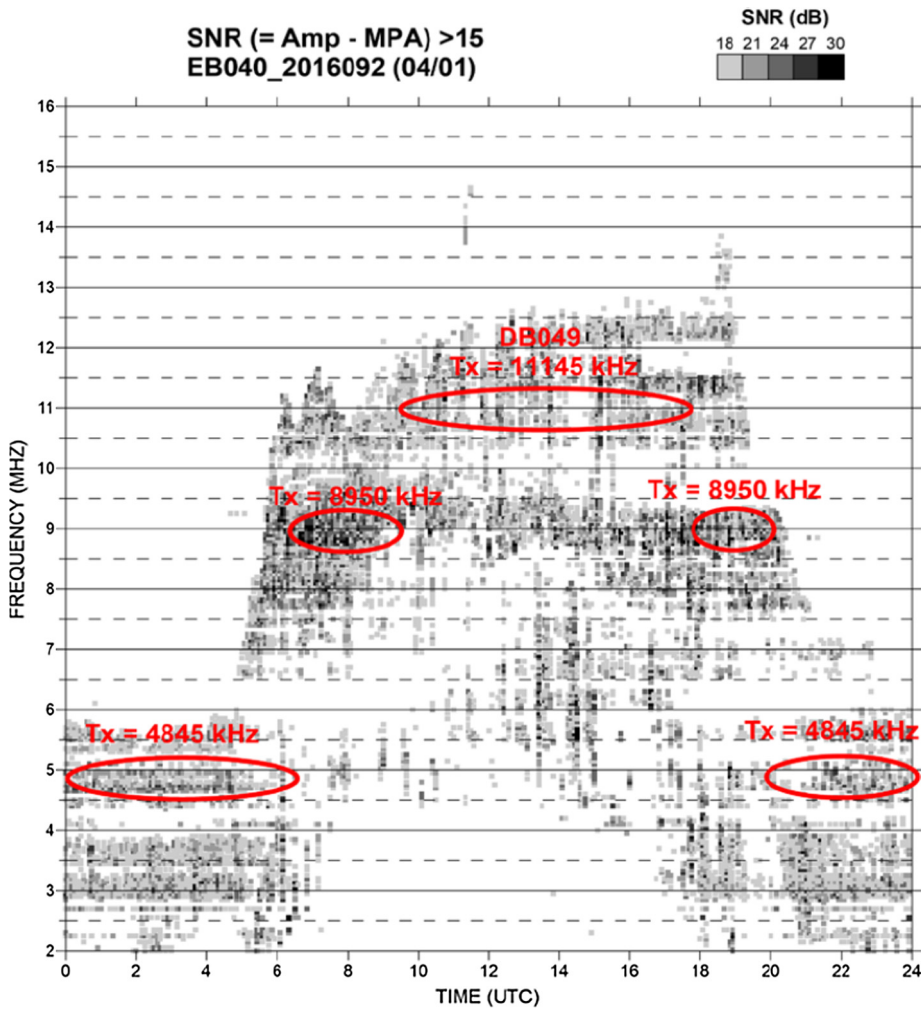


Fig. 5. Signal-to-noise ratios for the OI ionogram signals received at Ebre with transmissions from Dourbes.

of the measured data (Reinisch et al., submitted for publication), and every switching of the sounding frequency interrupts the analysis, leading to loss of potential TID data. In January 2017, it was therefore decided to

operate with just two frequencies, one for daytime and one for night-time. The night-time ↔ daytime switching times as well as the selection of the optimum sounding frequencies is periodically adjusted to accommodate the sea-

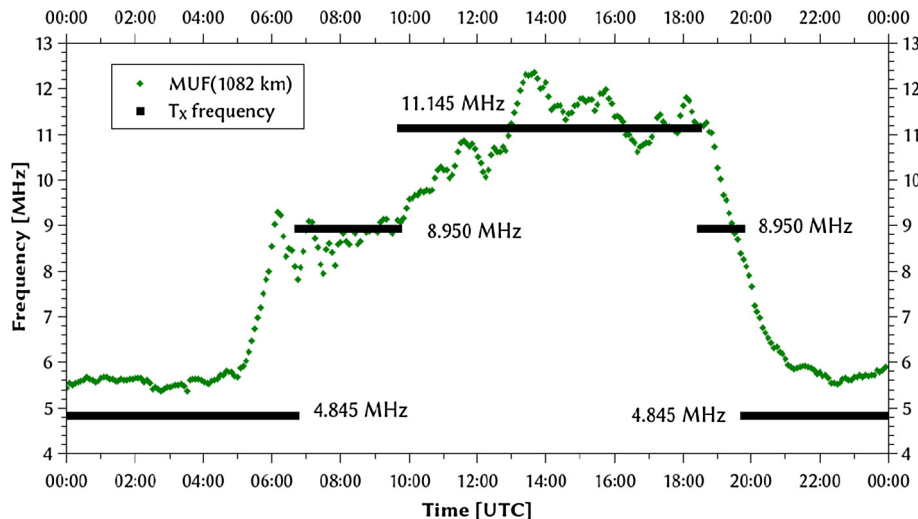


Fig. 6. D2D sounding frequencies (black) used on the Dourbes-to-Ebre path for 1 April 2016 and the MUF automatically scaled from the VI ionograms at Ebre.

sonal variations in the ionosphere. These updates are currently made every few weeks during equinox months, when sunrise and sunset times change quickly, and monthly during the winter and summer seasons.

Daily charting of the stepped-frequency SNR of OI sounding (Fig. 5) offers the potential for a fully automatic frequency management of the fixed-frequency D2D transmissions, thus sparing the tedious effort of manually selecting and commanding optimal frequencies at both ends of the D2D link. Most of the components required for such automatic system are already in place (Reinisch et al., 2004; Khmyrov et al., 2008). An Automatic Data Request and Execution Subsystem (ADRES) at the Lowell GIRO Data Center (LGDC), <http://ulcar.uml.edu/DIDBase/> has the capability of delivering Remote Campaign Requests (RCRs) to Digisondes to switch their operation parameters. The ADRES was originally designed to command GIRO Digisondes into the high-cadence sounding mode during co-incident overflights of DMSP spacecraft. ADRES will be adapted to distributing the selected frequencies and frequency switching times to the network Digisondes. Algorithms for the statistical analysis of the SNR charts (Fig. 5) and the diurnal MUF variations (Fig. 6) need to be developed.

Fig. 6 compares the MUF frequencies (green<sup>1</sup>), derived from the measured vertical EDPs at Ebre for the Dourbes-to-Ebre link, with the sounding frequencies (black) that had been manually pre-set for 1 April 2016 based on statistical evaluations of the SNR measurements.

During magnetically disturbed days the sounding frequencies may need to be lowered because the quiet-time sounding frequencies are no longer supported by the disturbed ionosphere, as illustrated by the SNR variations in Fig. 7 for two consecutive days in October 2015. Quiet

conditions prevailed during 6 October (left panel) until ~22 UT when the effects of a magnetic storm, which reached a minimum *Dst* value of -124, reduced the MUF by about 1 MHz. During the entire following day (Fig. 7, right panel) the MUF for the Dourbes-to-Ebre link the MUF was low by ~1 MHz. The nominal D2D sounding frequencies, 8.950 MHz during daytime and 4.845 MHz during night-time were clearly too high, and no useful D2D fixed-frequency OI signals were received at Ebre for the entire day.

### 3.2. Oblique sounding Dourbes to Athens

Since May 2016, attempts have been made to receive oblique signals from the Dourbes transmitter at Ebre and Athens simultaneously, both in the form of OI ionograms and fixed-frequency skymap soundings. These experiments have been partially successful. D2D signals optimised for the Dourbes to Ebre link have sometimes been recorded at Athens as well, but not systematically at all times. Oblique traces in the Athens ionograms have also been recorded, but not with the same SNR as in Ebre.

Various factors can be identified that contribute to the difficulty of performing oblique soundings on both paths at the same time. In Fig. 8 the SNR for all measured frequencies throughout one day, 9 February 2017, are shown for both Ebre (left panel) and Athens (right panel). This plot shows the SNR for both the vertical and oblique echoes. The echoes received below about 4 MHz during night-time and below 7 MHz during day-time are from the vertical reflections, the echoes at higher frequencies are reflections of the Dourbes signal. It is clear that the vertical echoes at each location generally have a higher SNR than the oblique traces. However, it is also immediately evident that the SNR for the vertical echoes in Athens is significantly lower than in Ebre, especially during the day-time. This is the result of the technical characteristics of

<sup>1</sup> For interpretation of color in 'Figs. 3 and 6', the reader is referred to the web version of this article.

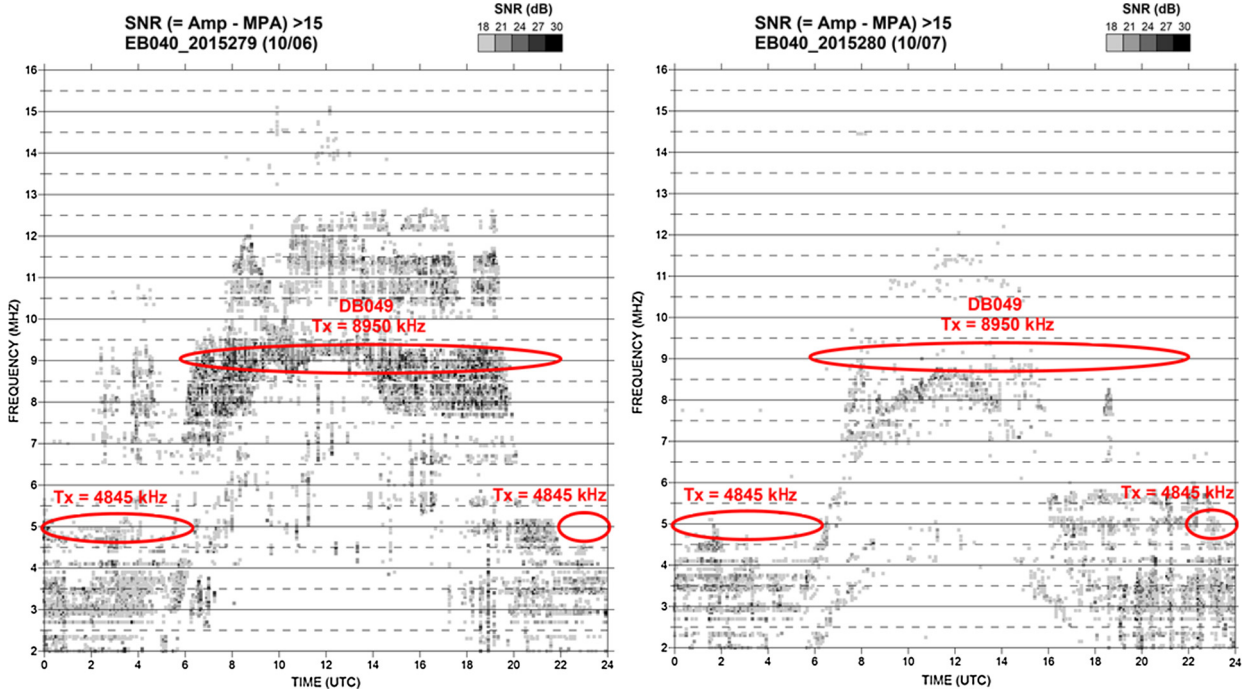


Fig. 7. The effect of storm condition on the usability of selected D2D frequencies. The left panel shows the quiet time SNR (6 October 2015), the right panel shows the disturbed situation (7 October 2015).

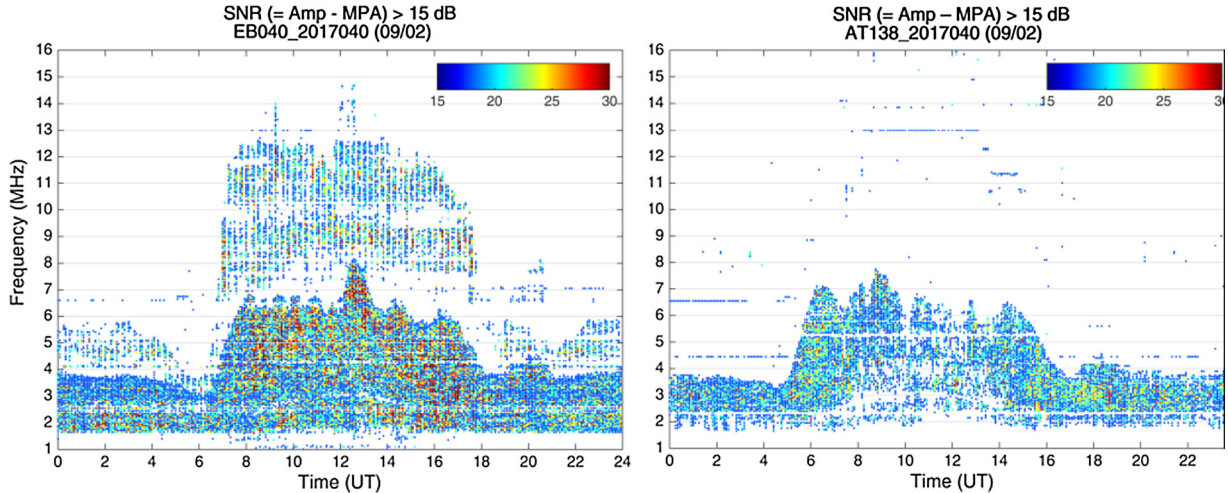


Fig. 8. Signal-to-noise ratio of the signals obtained in Ebre (left) and Athens (right) for 9 February 2017. These plots show the SNR of both the VI and the OI signals.

the antennas and the level of radio noise in the environment at each site. The generally lower SNR in Athens results in the oblique traces being only sporadically visible.

A second factor of importance for the oblique soundings SNR is the radiation pattern of the transmit antennas. Fig. 9 shows the antenna gain at various frequencies and elevations from the transmit antenna of the Dourbes observatory in the directions  $198^\circ$ , along the path to Ebre, and  $123^\circ$ , along the path to Athens. These gains were obtained by modelling the Dourbes transmit antenna with 4nec2, a NEC (Numerical Electromagnetics Code) based antenna

modeller and optimizer software (<http://www.qsl.net/4nec2/>). The vertical line indicates a typical transmission frequency of 8.95 MHz (see Figs. 7 and 8) while the horizontal lines indicate typical elevation angles for soundings on the paths from Dourbes to Ebre and Athens. At elevation angles close to  $90^\circ$ , the gain at all frequencies is the same in both directions. This corresponds to a uniform azimuthal radiation pattern close to the vertical direction. However, it is evident from Fig. 9 that, at lower elevation angles, for most frequencies the gain in the  $123^\circ$  direction is lower than in the  $198^\circ$  direction. This is a result of the

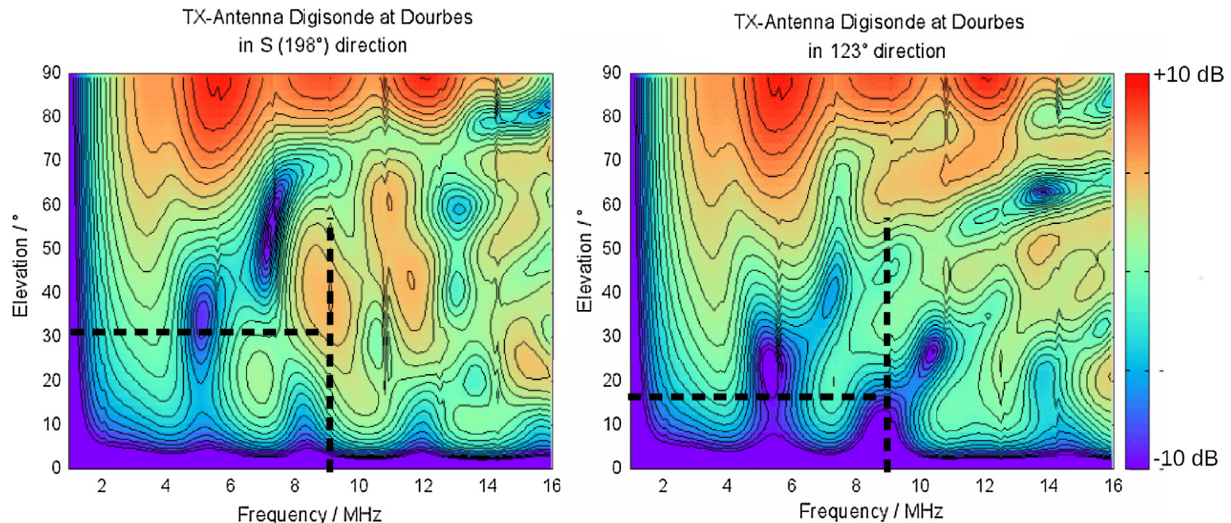


Fig. 9. Directional gain of the Dourbes transmit antenna in the direction of Ebrie (left) and Athens (right) as a function of frequency and elevation angle.

construction of the transmission antenna, which consists of two crossed delta antennas oriented in the North–South and East–West directions and produces side lobes that are not uniform for all azimuths. The  $198^\circ$  direction is closely aligned to one of the directions with the highest transmission gain of the side lobe responsible for the oblique transmission, while the  $123^\circ$  is close to the direction of a minimum in the gain. The peculiarities of the gain shown in Fig. 9 can result in unexpected loss of the oblique trace in Athens when optimising the D2D frequency for reception in Ebrie. For example, a frequency around 8.95 MHz would hit a local maximum in the gain at elevation angles around  $30^\circ$  in the  $198^\circ$  direction, but these frequencies coincide with a minimum in the gain in the  $123^\circ$  direction at the relevant elevation angles.

Fig. 9 shows significantly lower antenna gain for low elevation angles than at higher elevation angles. Because the path between Dourbes and Athens is about twice as long as that between Dourbes and Ebrie, the elevation angles on the former are much lower.

Besides the technical difficulties of simultaneous oblique soundings on both paths, it is important to keep in mind that the ionospheric conditions can be quite different between them. Both receiving stations are at similar latitude, but are separated by  $23^\circ$  in longitude. This means that during some parts of the year the times sunrise and sunset in Dourbes are closer to those in Ebrie, and at other times closer to those in Athens (see Fig. 10). Because the frequency switching times are optimised for the Dourbes to Ebrie path, these seasonal differences cause additional periods during which reception in Athens might be impossible.

#### 4. TID signatures observed in Doppler shift

Although the primary intention of the Net-TIDE project was to provide Doppler frequency and angle of arrival measurements for use with the FAS technique for the detection and specification of TIDs, it is also possible to

estimate some TID parameters directly from the Doppler frequency variations (Chum et al., 2010; Altadill et al., submitted for publication). Fig. 11 shows the Doppler frequency measured during four days in October 2015. At the time of these measurements the soundings on the Dourbes to Ebrie path were done using two frequencies: a 8.950 MHz daytime frequency from 07 UT to 22 UT, and a night-time frequency of 4.845 MHz between 22 UT and 07 UT. It is evident from the figure that there are periods around sunrise and sunset when no oblique signals could be received. However, for the rest of the day, the Doppler frequency can be reliably measured. During the day, variations of the Doppler frequency are insignificant, but during the nights some oscillatory behaviour can be seen. Such oscillations can be seen in all the nights presented in Fig. 11, but is most obvious between 22 UT and 00 UT on 12 and 13 October. These oscillatory patterns have periods of about twenty minutes to one hour, corresponding to the established range of periods of medium-scale TIDs. The consistent negative bias in the Doppler data is the result a slight difference in the sounding frequencies at the two stations, the Dourbes frequency being larger by  $\sim 1$  part in  $5 \times 10^6$ . In Fig. 12, the MUF obtained from the vertical soundings at each end of the path is shown for this night, together with the Doppler frequency. Since the two end-points of the signal path and the reflection point are collinear, a phase shift is expected between the observations at the different points if one assumes the TID moves without changes and travels in the direction of the link in the Net-TIDE network. From this phase shift, it is possible to determine the phase velocity  $v_\phi$  and wavelength  $\lambda$  of the TID (see the appendix for the details of this calculations). We find that in this case the time between observing the minima in the MUF at both stations is about 25 min, so for this TID the component of  $v_\phi$  in the direction of the path from Dourbes to Ebrie is 723 m/s. Notice that this is only an upper bound on the TID velocity, as explained in the appendix, and the real

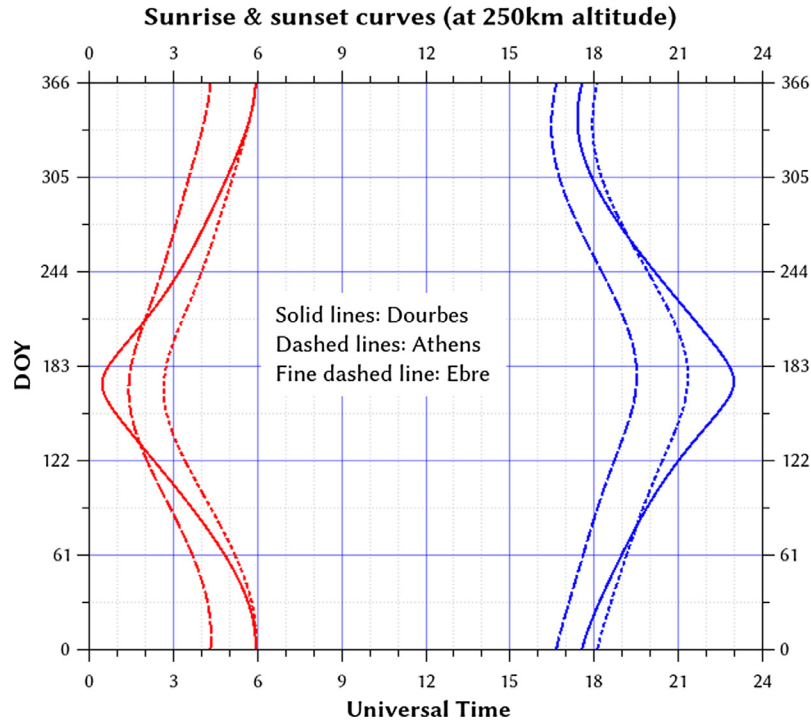


Fig. 10. Variations of the times of sunrise and sunset at 250 km altitude during the year at Dourbes, Ebre and Athens.

velocity might be lower. An analysis of this TID using different methodologies will be presented in the forthcoming paper by Altadill et al. (submitted for publication).

## 5. Discussion and possible further improvements

Over the course of these experiments in oblique soundings, some technical issues have arisen, and some possible improvements in both hardware and software have become clear. Currently, the frequency used for D2D soundings has to be selected by manual inspection of the signal-to-noise ratios of the OI signals in the oblique ionograms. The switching of the transmitting and receiving stations to a newly selected D2D frequency is also done manually by the Digisonde operators. This imposes some limitations on how quick the network can be adapted to changing ionospheric conditions, for example in reaction to a geomagnetic storm. In the future, these processes of selecting an appropriate sounding frequency and updating the Digisonde programming could be automated. The Digisonde already provides the possibility of being reprogrammed remotely by using Remote Campaign Requests, but this system is intended for campaigns of fixed duration and needs to be adapted for use with an operational monitoring network. The D2D sounding frequencies can be selected based on parameters that are automatically scaled from the vertical ionograms, e.g., the MUF or critical frequency at the receiving station, or by automatically scaling some parameter from the oblique ionogram traces. A similar operational algorithm has recently been activated on the Pruhonice-to-Juliusruh path (517 km). The MUF600 is

routinely scaled automatically from the Juliusruh VI ionograms, and the D2D frequency is automatically lowered to a predefined “storm time” value when the MUF600 falls below the regular D2D frequency.

Another important issue from an operational point of view is the need of a minimal period (currently 160 min) of soundings on a fixed frequency to be available in order to apply the FAS technique. This implies that the amount of frequency changes over the course of a day should be kept to a minimum, and that any such change will cause the FAS based TID detection technique to be unavailable for some time. This issue could be resolved by performing D2D soundings on multiple frequencies at the same time, so that before any switch between frequencies an overlap period can be introduced in the schedule during which data on the new frequency can be collected while the old one is still used to provide input to the FAS analysis. Simultaneous D2D soundings on multiple frequencies are currently not possible, but this capability can be provided by new Digisonde software.

A significant increase in the number of sounding paths, and thus in the data available for FAS analysis, could come from having multiple Digisonde stations act as simultaneous receivers for a single transmitting station. However, there are some additional problems that can arise when performing D2D soundings on different paths at the same time. One issue is that the frequency chosen for such operations has to be low enough to be usable on the shortest path, meaning it should be below the MUF for this distance. The nondeative absorption at these frequencies might impede reception over the longer distances.

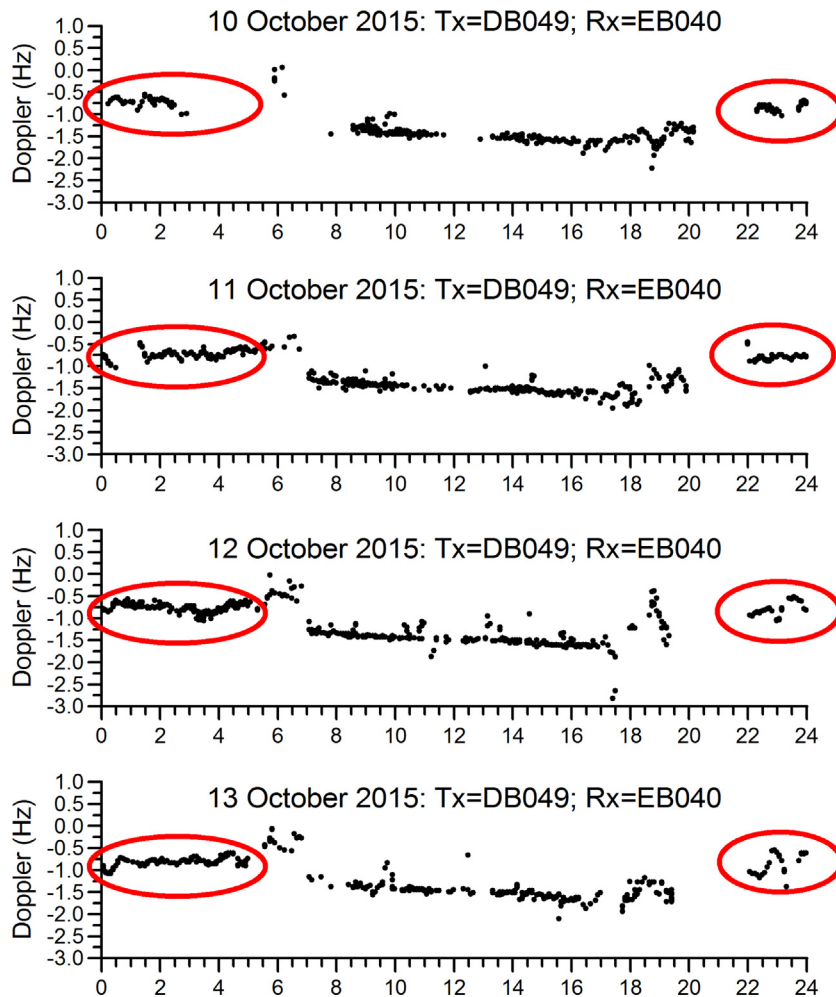


Fig. 11. D2D Doppler shift on the Dourbes to Ebre path for 10–13 October 2015.

Also the design of the transmission antennas plays an important role. The various ionospheric observatories involved in this project are equipped with antennas primarily intended for vertical sounding. For the low elevation angles involved in long distance oblique sounding, the gain of these antennas is much lower than in the vertical direction. Additionally, the gain of the transmit antennas is not the same in all directions. The planned future use of multiplexed transmission at several fixed frequencies will likely reduce some of these problems. Alternatively, dedicated antennas designed for oblique sounding could greatly improve the SNR that is obtainable.

Despite the challenges encountered during this project, high quality data were obtained from the D2D soundings. Once the data has been processed using the clustering and tracking algorithms, they can be used in the FAS analyses for TID detection (Reinisch et al., submitted for publication). Alternatively, a simpler analysis can be done as described in the preceding section. This method of detecting TIDs has the advantage of being computationally easier than the FAS technique, but has some other limitations. Apart from the various assumptions described in the

appendix, this method enables detection only of the component of the velocity along the direction of the path of the oblique soundings. Nevertheless, the values obtained in this case study correspond well to those found using different methods of analysis, indicating that the proposed method can indeed be used at least to determine a TID's velocity component in the direction of the sounding path.

## 6. Conclusions

The Net-TIDE project has resulted in the collection of about two years of data produced by oblique ionosonde soundings between various European Digisonde stations. Various schedules have been experimented with for both combined vertical and oblique soundings, and for single frequency D2D soundings. Over the course of these experiments, various challenges have become evident, especially in the cases when oblique soundings are executed over long distances. Nevertheless, at the beginning of 2017 a stable network has been established that delivers data on a regular schedule for use in the FAS technique for the detection of travelling ionospheric disturbances.

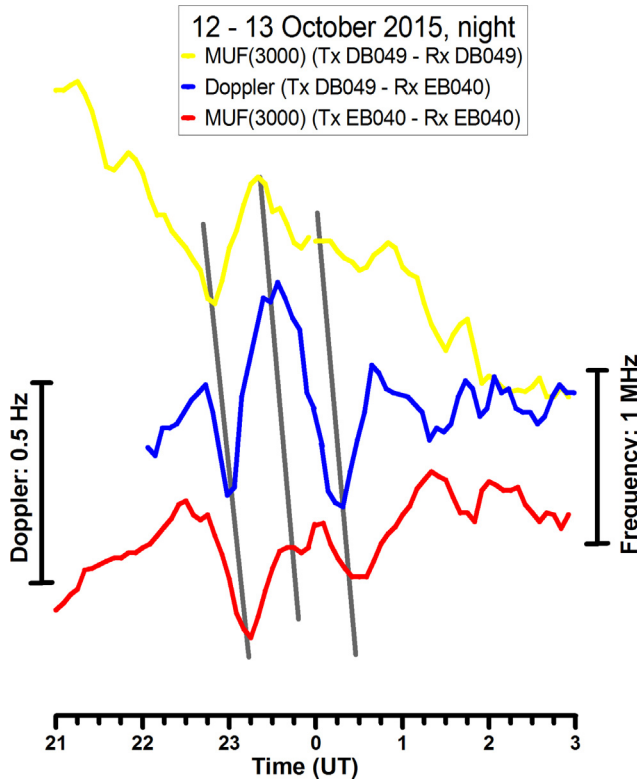


Fig. 12. MUF(3000) measured at Dourbes (yellow) and Ebre (red), and the Doppler shift obtained from D2D soundings (blue) during the night from 12 to 13 October 2015. (For interpretation of the references to colour in this figure legend, the reader is referred to the web version of this article.)

The data that are currently being collected in the TID monitoring network are of sufficient quality to be used in the detection of TIDs, whether by the FAS technique or by the method described in this paper. The principle issue is in the assured coverage of the observations of both time and space. Around sunrise and sunset, a changing of the frequency used for producing D2D skymaps is unavoidable, resulting in a gap in the TID monitoring around these times. Additional gaps in data sets could appear in consequence of geomagnetic storms or radio interference. These problems can in the future be solved by improvements of the hardware and software of the Digisondes. For the spatial coverage of Europe, it is important to add additional links to the monitoring network. This can either be done by establishing a system with multiple receivers recording oblique signals from a single transmitter, or by adding more observatories to.

#### Acknowledgements

This work is supported by the NATO Science for Peace and Security project #984894. T. Verhulst and S. Stankov are supported by the Royal Meteorological Institute (RMI) via the Belgian Solar-Terrestrial Centre of Excellence (STCE). B. Reinisch, I. Galkin, and V. Paznukhov were in part supported by AFRL's SBIR project #FA9453-14-

C-0305, and by subcontract from SwRI under project FA8650-16-C-9104. D. Altadill and E. Blanch are supported by Universitat Ramon Llull projects 2016-URL-Trac-001 and 2016-URL-Internac-027 supported by “Obra Social la Caixa”, and 2016-URL-IR-001 supported by “Generalitat de Catalunya”, D. Burešová is supported by the Czech Science Foundation via Grant 15-07281J. We acknowledge access to the Global Ionospheric Radio Observatory (GIRO) databases at the Lowell GIRO Data Center (LGDC), <http://giro.uml.edu/>.

#### Appendix A

This appendix contains the calculation of the phase delay between the extrema caused by a TID in the *MUF* derived from the vertical incidence soundings at an ionosonde station and the Doppler shift observed in D2D soundings between the stations. The electron density  $N(h, t)$  as a function of time and altitude at an ionosonde  $S$  in the presence of a TID is given by:

$$N^S(h, t) = N_0^S(h)(1 + A \cos(\omega t)) \quad (\text{A1})$$

where  $N_0^S(h)$  is the undisturbed electron density profile,  $A$  is the amplitude of the disturbance and  $\omega$  is the radial frequency. The same TID observed at a different station  $S'$ , a distance  $2d$  away from the first, is described by:

$$N^{S'}(h, t) = N_0^{S'}(h) \left( 1 + A \cos \left( \omega t - \frac{2\omega d}{v} \right) \right) \quad (\text{A2})$$

At the reflection point  $R$  halfway between the two ionosondes, the electron density is then given by:

$$N^R(h, t) = N_0^R(h) \left( 1 + A \cos \left( \omega t - \frac{\omega d}{v} \right) \right) \quad (\text{A3})$$

with  $d$  the distance from the ionosonde to the reflection point and  $v$  the velocity of the TID. We assume that the undisturbed electron density profile is identical at both locations, and denote it by  $N_0(h)$ .

The *MUF* observed at the sounding station  $S$  is (with some constant  $C$ )

$$MUF^S(t) = C \sqrt{N^S(h_m F_2, t)} \quad (\text{A4})$$

Thus, the extrema in the *MUF* will be observed whenever

$$\frac{dMUF^S(t)}{dt} = 0 = \frac{-C}{2\sqrt{N^S(h_m F_2, t)}} A \omega \sin(\omega t) \quad (\text{A5})$$

Exactly the same calculation can be done for the *MUF* at stations  $S'$ . Therefore, from the time delay between the observations of the minima and maxima of the *MUF*, the velocity component of the TID along the line between the two stations can be calculated immediately as  $v = \Delta t / 2d$ . Note that this speed will generally be too high. The real speed of the TID is equal to the one calculated

here multiplied by the cosine of the angle between the TID propagation direction and the line between the two observatories where the *MUF* was measured.

In order to calculate the times of the extrema observed in the Doppler shift, we will assume that the undisturbed density profile is parabolic:

$$N_0(\delta) = N_0 \delta^2 \quad (\text{A6})$$

where  $\delta$  is the distance below the peak altitude  $h_m F_2$ . Thus, Eq. (A2) becomes

$$N^R(\delta, t) = N_0 \delta^2 \left( 1 + A \cos \left( \omega t - \frac{\omega d}{v} \right) \right) \quad (\text{A7})$$

The Doppler shift  $\Delta f$  for a transmission frequency  $f_T$  is

$$\Delta f = 2 \frac{v_r}{c} f_T \quad (\text{A8})$$

and the radial velocity of the reflecting medium. The latter is equal to

$$v_r = \cos \zeta \frac{d\delta(N_f, t)}{dt} \quad (\text{A9})$$

where  $\zeta$  is the zenith angle of the observed reflection,  $N_f$  is the plasma density reflecting the frequency  $f$  and  $\delta(N_f, t)$  is the distance below the peak at which this density occurs. This distance can be obtained from inverting Eq. (A6):

$$\delta(N_f, t) = \sqrt{\frac{N_f}{N_0 \left( 1 + A \cos \left( \omega t - \frac{\omega d}{v} \right) \right)}} \quad (\text{A10})$$

The Doppler shift can now be obtained by combining Eqs. (A7) and (A9):

$$\Delta f = \frac{f}{c} \cos \zeta \sqrt{\frac{N_f}{N_0}} \frac{A \omega \sin \left( \omega t - \frac{\omega d}{v} \right)}{\left( 1 + A \cos \left( \omega t - \frac{\omega d}{v} \right) \right)^{\frac{3}{2}}} \quad (\text{A11})$$

Thus, the extrema in the Doppler shift occur whenever

$$\frac{d\Delta f}{dt} = 0 = \frac{f \cos \zeta}{2c} A \omega^2 \left( \frac{\cos(\omega t - \frac{\omega d}{v})}{\left( 1 + A \cos(\omega t - \frac{\omega d}{v}) \right)^{\frac{3}{2}}} + \frac{3}{2} A \frac{\sin^2(\omega t - \frac{\omega d}{v})}{\left( 1 + A \cos(\omega t - \frac{\omega d}{v}) \right)^{\frac{5}{2}}} \right) \quad (\text{A12})$$

If the amplitude of the TID is small, the second order contribution in Eq. (A11) can be neglected and the extrema in the Doppler shift occur whenever

$$\cos \left( \omega t - \frac{\omega d}{v} \right) = 0 \quad (\text{A13})$$

From (A4) and (A12) it can be seen that the time delay  $\Delta t$  between the extrema observed in the *MUF* and  $\Delta f$  is given by

$$\Delta t = \frac{\frac{1}{2}(n + \frac{1}{2})\lambda + d}{v} \quad (\text{A14})$$

where  $\lambda$  is the wavelength of the TID. Notice that the wavelength calculated here is only an approximation. As was mentioned before in the context of the speed calculation, these calculations are done assuming the TID propagates in the direction of the line connecting the ionosonde observatories.

## References

- Afraimovich, E.L., Kosogorov, E.A., Leonovich, L.A., Palamartchouk, K.S., Perevalova, N.P., Pirog, O.M., 2000. Determining parameters of large-scale traveling ionospheric disturbances of auroral origin using GPS-arrays. *J. Atmos. Sol.-Ter. Phys.* 62, 553–565.
- Afraimovich, E.L., Voeykov, S.V., Perevalova, N.P., Ratovsky, K.G., 2008. Large-scale traveling ionospheric disturbances of auroral origin according to the data of the GPS network and ionosondes. *Adv. Space Res.* 42, 1213–1217.
- Altadill, D., Blanch, E., Paznukhov, V., Miguel Juan, J., Belehaki, A., Verhulst, T., Galkin, I., Reinisch, B., Buresova, D., Mielich, J., Parkinson, M., Sanz, J., 2017. Identification of travelling ionospheric disturbances applying interferometry analysis to classical ionogram data from an ionosonde network. *IEEE Trans. Geosci. Rem. Sens.* (submitted for publication).
- Astafyeva, E.I., Afraimovich, E.L., 2004. Long-distance traveling ionospheric disturbances caused by the great Sumatra-Andaman earthquake on 26 December 2004. *Earth Planets Sp.* 58, 1025–1031, 2006.
- Balthazar, R.L., Moffett, R.J., 1997. A study of atmospheric gravity waves and travelling ionospheric disturbances at equatorial latitudes. *Ann. Geophys.* 15, 1048–1056.
- Belehaki, A., Reinisch, B., Galkin, I., Altadill, D., Buresova, D., Francis, M., Mielich, J., Paznukhov, V., Stankov, S., 2015. Pilot network for identification of travelling ionospheric disturbances. In: Proc. 14th Int. Ionospheric Effects Symposium (IES-2015), Alexandria, Virginia, 12–14 May 2015, pp. 248–256, <http://ies2015.bc.edu/wp-content/uploads/2015/08/IES2015-Proceedings.pdf>.
- Bilitz, D., Altadill, D., Zhang, Y., Mertens, C., Truhlik, V., Richards, P., McKinnell, L.A., Reinisch, B., 2014. The international reference ionosphere 2012 – a model of international collaboration. *J. Space Weather Space Clim.* 4, A07. <http://dx.doi.org/10.1051/swsc/2014004>.
- Borries, C., Jakowski, N., Wilken, V., 2009. Storm induced large scale TIDs observed in GPS derived TEC. *Ann. Geophys.* 27, 1605–1612. <http://dx.doi.org/10.5194/angeo-27-1605-2009>.
- Chum, J., Šindelářová, T., Lastovička, J., Hruška, J., Burešová, D., Baše, J., 2010. Horizontal velocities and propagation directions of gravity waves in the ionosphere over the Czech Republic. *J. Geophys. Res.* 115, A11322. <http://dx.doi.org/10.1029/2010JA015821>.
- Davies, K., 1990. *Ionospheric Radio*. Peter Peregrinus Ltd., London, UK.
- de Boer, P.-T., 2013. Chirp Reception and Interpretation, PA3FWM. <<http://websdr.ewi.utwente.nl:8901/chirps/article/>>.
- Ding, F., Wan, W., Ning, B., Wang, M., 2007. Large-scale travelling ionospheric disturbances observed by GPS total electron content during the magnetic storm of 29–30 October 2003. *J. Geophys. Res.* 112, A06309. <http://dx.doi.org/10.1029/2006JA012013>.
- Frissell, N.A., Baker, J.B.H., Ruohoniemi, J.M., Gerrard, A.J., Miller, E.S., Marini, J.P., West, M.L., Bristow, W.A., 2014. Climatology of medium-scale traveling ionospheric disturbances observed by the midlatitude Blackstone SuperDARN radar. *J. Geophys. Res.* 119, 7679–7697. <http://dx.doi.org/10.1002/2014JA019870>.
- Galkin, I.A., Khmyrov, G.M., Kozlov, A.V., Reinisch, B.W., Huang, X., Paznukhov, V.V., 2008. The ARTIST 5, in radio sounding and plasma physics. *AIP Conf. Proc.* 974, 150–159.
- Galushko, V.G., Beley, V.S., Koloskov, A.V., Yampolski, Y.M., Paznukhov, V.V., Reinisch, B.W., Foster, J.C., Erickson, P., 2003. Frequency-and-angular HF sounding and ISR diagnostics of TIDs. *Radio Sci.* 38 (6), 1102.
- Hernández-Pajares, M., Juan, J.M., Sanz, J., 2006. Medium-scale travelling ionospheric disturbances affecting GPS measurements: spatial and temporal analysis. *J. Geophys. Res.* 111, A07S11. <http://dx.doi.org/10.1029/2005JA011474>.
- Hines, C.O., 1974. *The Upper Atmosphere in Motion*. Geophysical Monograph, American Geophysical Union, Washington, DC.
- Ho, C.M., Iijima, B.A., Lindqvist, X.P., Mannucci, A.J., Sparks, L., Reyes, M.J., Wilson, B.D., 1998. Ionospheric total electron content perturbations monitored by the GPS global network during two

- northern hemisphere winter storms. *J. Geophys. Res.* 103, 26409–26420.
- Hocke, K., Schlegel, K., 1996. A review of atmospheric gravity waves and travelling ionospheric disturbances: 1982–1995. *Ann. Geophys.* 14, 917. <http://dx.doi.org/10.1007/s00585-996-0917-6>.
- Huang, X., Reinisch, B.W., Sales, G.S., Paznukhov, V.V., Galkin, I.A., 2016. Comparing TID simulations using 3-D ray tracing and mirror reflection. *Radio Sci.* 51, 337–343. <http://dx.doi.org/10.1002/2015RS005872>.
- Hunsucker, R.D., 1982. Atmospheric gravity waves generated in the high-latitude ionosphere: a review. *Rev. Geophys. Space Phys.* 20 (2), 293–315.
- Khmyrov, G.M., Galkin, I.A., Kozlov, A.V., Reinisch, B.W., McElroy, J., Dozois, C., 2008. Exploring digisonde ionogram data with SAO-X and DIDBase. *Radio Sounding and Plasma Physics, AIP Conf. Proc.*, vol. 974, pp. 175–185.
- Krasheninnikov, I.V., Jodogne, J.-C., Alberca, L.F., 1996. Compatible analysis of vertical and oblique ionospheric sounding data. *Ann. Geofis.* XXXIX (4), 763–768.
- Lakshmi Narayanan, V., Shiokawa, K., Otsuka, Y., Saito, S., 2014. Airglow observations of nighttime medium-scale traveling ionospheric disturbances from Yonaguni: statistical characteristics and low-latitude limit. *J. Geophys. Res.* 119, 9268–9282. <http://dx.doi.org/10.1002/2014JA020368>.
- LDI, 2014. DPS-4D Operation Manual v1.2.6. <<http://www.digisonde.com/dps-4dmanual.html>>.
- MacDougall, J., Abdu, M.A., Batista, I., Fagundes, P.R., Sahai, Y., Jayachandran, P.T., 2009. On the production of travelling ionospheric disturbances by atmospheric gravity waves. *J. Atmos. Sol.-Terr. Phys.* 71, 2013–2016.
- Otsuka, Y., Shiokawa, K., Ogawa, T., Yokoyama, T., Yamamoto, M., 2009. Spatial relationship of nighttime medium-scale traveling ionospheric disturbances and F region field-aligned irregularities observed with two spaced all-sky airglow imagers and the middle and upper atmosphere radar. *J. Geophys. Res.* 114, A05302. <http://dx.doi.org/10.1029/2008JA013902>.
- Paznukhov, V.V., Galushko, V.G., Reinisch, B.W., 2012. Digisonde observations of AGWs/TIDs with frequency and angular sounding technique. *Adv. Space. Res.* 49 (4), 700–710. <http://dx.doi.org/10.1016/j.asr.2011.11.012>.
- Pintor, P., Roldán, R., Gómez, J., de la Casa, C., Fidalgo, R.M., 2015. The impact of the high ionospheric activity in the EGNOS performance. *Coordinates Mag.* XI (03), 20–28.
- Reinisch, B.W., Galkin, I., Belehaki, A., Paznukhov, V., Huang, X., Mielich, J., Altadill, D., Buresova, D., Verhulst, T., Stankov, S., Blanch, E., Kouba, D., Hamel, R., Kozlov, A., Tsagouri, I., Mouzakis, A., Messerotti, M., Parkinson, M., Ishii, M., 2017. Pilot network for identification of travelling ionospheric disturbances, *Radio Sci.* (submitted for publication).
- Reinisch, B.W., Galkin, I.A., Khmyrov, G.M., et al., 2009. The new Digisonde for research and monitoring applications. *Radio Sci.* 44, RS0A24. <http://dx.doi.org/10.1029/2008RS004115>.
- Reinisch, B.W., Galkin, I.A., Khmyrov, G., Kozlov, A., Kitrosser, D.F., 2004. Automated collection and dissemination of ionospheric data from the digisonde network. *Adv. Radio Sci.* 2, 241–247.
- Reinisch, B.W., Bibl, K., Ahmed, M., Soicher, H., Gorman, F., Jodogne, J.-C., 1984a. Multipath and Doppler observations during transatlantic digital HF propagation experiments. In: Blythe, J.H. (Ed.), *Propagation Influences on Digital Transmission Systems—Problems and Solutions (Proc. NATO AGARD Conference, 4–8 June 1984, Athens, Greece)*, Ed. NATO Conference Proceedings No. AGARD-CP-363, pp. (12)1–(12)10.
- Reinisch, B.W., Ahmed, M., Bibl, K., Soicher, H., Gorman, F., Jodogne, J.C., Bossy, L., King, J., Gilbert, J., 1984b. A transatlantic digital HF radio link experiment. In: Proc. Ionospheric Effects Symposium (IES), 1–3 May 1984, Alexandria VA, USA, pp. 111–122.
- Reinisch, B.W., Huang, X., 1983. Automatic calculation of electron density profiles from digital ionograms, 3, processing of bottomside ionograms. *Radio Sci.* 18, 477–492.
- Zolesi, B., Fontana, G., Perrone, L., Pietrella, M., Romano, V., Tutone, G., Belehaki, A., Tsagouri, I., Kouris, S.S., Vallianatos, F., Makris, J. P., Angling, M.J., 2008. A new campaign for oblique-incidence ionospheric sounding over Europe and its data application. *J. Atmos. Sol.-Terr. Phys.* 70, 854–865. <http://dx.doi.org/10.1016/j.jastp.2007.02.015>.